DESIGN OF A RING RF SYSTEM

D. Boussard*)
CERN, Geneva, Switzerland

ABSTRACT

In a circular accelerator or collider, the excitation of coherent longitudinal oscillations (dipole and quadrupole) by RF noise, magnetic fluctuations and the like may cause indesirable effects, for instance emittance blow-up or even beam losses. The RF system architecture can be designed to damp these oscillations using feedback techniques. These will be presented in this paper, both for the low intensity case and when cavity beam loading becomes important.

1. INTRODUCTION

Conceptually the radiofrequency system of a circular accelerator or collider is, at first sight, very simple. The accelerating cavity which acts on the beam is driven by an RF power amplifier. The amplitude of the accelerating voltage is adjusted with a modulator (assumed linear), and its frequency (which must be programmed according to the desired radial position, for a given bending field) is controlled with a frequency generator (Fig.1). Despite large variations in the technical solutions adopted (different frequency ranges, different RF powers and voltages) this basic scheme applies to most ring type machines.

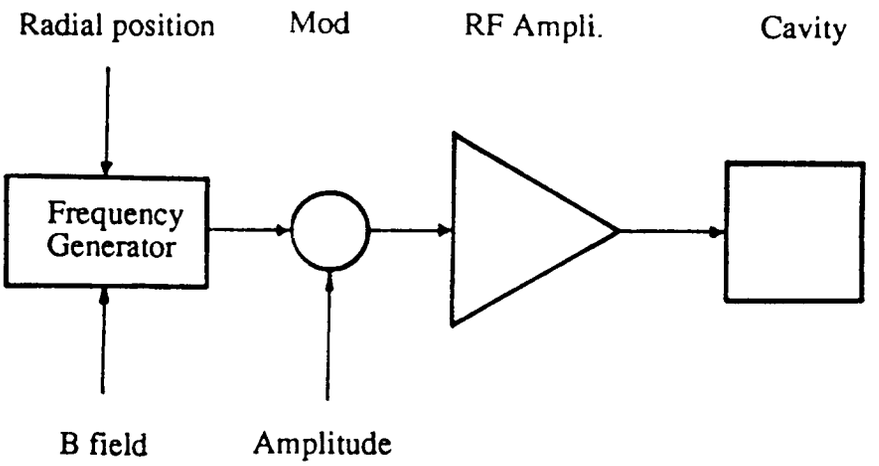

Fig. 1 The simplest RF system

However, in many cases such a simple arrangement is inadequate, because it is sensitive to errors, the most common being for instance:

- fluctuations of the magnetic field
- phase errors at injection of a bunched beam
- RF noise in the frequency generator
- ripple in the RF power amplifiers.

The effects of these is to excite coherent longitudinal oscillations of the beam (dipole, quadrupole, etc) which ultimately may lead to emittance blow up and even beam losses. In

*) Lecture originally presented at the CAS Fourth General Accelerator Physics Course, Jülich, 1990 and published as CERN Yellow Report CERN 91-04. It is reproduced here in order that all topics covered in the RF Engineering for Particle Accelerators course appear under one cover.

electron machines, where natural damping is present, those effects may be neglected if they are weak enough. For hadron machines, on the contrary, there is no such damping; consequently the RF system must be designed to damp coherent longitudinal oscillations (dipole and quadrupole) in order to avoid uncontrolled emittance blow-up. The purpose of this lecture is to review the means to achieve this objective, first for low intensity beams, and thereafter, when cavity beam loading becomes important.

2. DIPOLE AND QUADRUPOLE MODE DAMPING AT LOW INTENSITY

2.1 Basic principle

To damp the dipole mode of oscillation we must introduce a friction term in the linearized synchrotron equation (for the center of gravity of the bunch):

$$\frac{d^2\phi}{dt^2} + \alpha\frac{d\phi}{dt} + \omega_s^2\phi = 0 \qquad (1)$$

ϕ : phase deviation with respect to the synchronous particle,

$\omega_s / 2\pi$: synchrotron frequency.

The damping term $\alpha\frac{d\phi}{dt} = j\omega\,\alpha\phi$ which is in quadrature with ϕ can be obtained if the original scheme of Fig. 1 is somewhat modified as in Fig. 2. The RF component of the beam is obtained with a pick-up electrode followed by a filter centered at the RF frequency. By measuring the relative RF phase between this beam signal and that of the frequency generator, one obtains the phase deviation ϕ (equation 1). In reality the measured phase deviation contains in addition a steady, or slowly varying offset due, for instance, to the delays in the measuring equipment or to the varying synchronous phase. Damping is achieved if the phase deviation signal, ϕ, is shifted by 90° at the synchrotron frequency (Fig. 2). The shifted-in-phase signal modifies the original RF via a controllable phase shifter inserted in the cavity drive chain. Such a system follows equation (1), in which α is proportional to the loop gain.

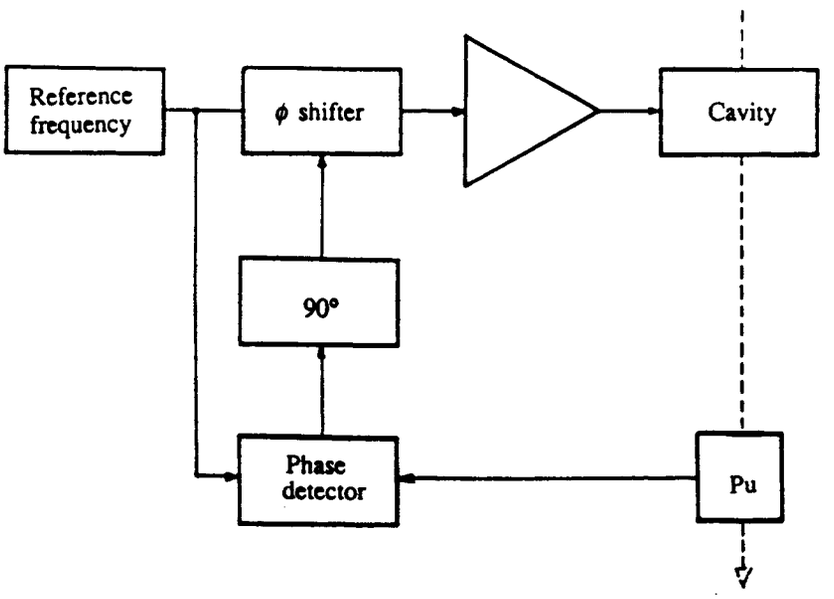

Fig. 2 Damping of the dipole mode

This is not the only conceivable scheme to damp coherent phase (dipole) oscillations. Instead of measuring the phase error, one can look at the energy deviation, in which case no 90° phase shift is needed in the feedback path. The energy deviation being proportional to radial displacement, can be measured with a radial pick-up electrode located in a region of large dispersion. In practice, there is a limited resolution in the radial measurement (betatron oscillations, noise, etc) which leads to rather small loop gains and slow damping.

2.2 Damping rate

The system of Fig. 2 can be conveniently analyzed using the concept of beam transfer function $B(s)$, defined as the ratio of beam phase p_B to cavity phase p_v (measured with respect to the RF reference). For small oscillations (linearized synchrotron equation):

$$\mathrm{B(s)} = \frac{\omega_s^{\,2}}{s^2 + \omega_s^{\,2}} \tag{2}$$

where s is the complex variable. As expected $B(s)$ has poles $s = \pm j\omega_s$ for the real frequency ω_s (no damping).

With the transfer function of the electronic feedback return path, $G(s)$ (from beam phase measurement to cavity phase), one obtains the characteristic equation of the system:

$$\mathrm{G(s)} \cdot \mathrm{B(s)} - 1 = 0 \quad . \tag{3}$$

In the simple (ideal) case $G(s) = G_0 \dfrac{s}{\omega_p}$ (pure differentiator) one obtains

$$s^2 - sG_0 \frac{\omega_s^2}{\omega_p} + \omega_s^2 = 0 \tag{4}$$

for which the two roots:

$$s_{1,2} = \pm j\omega_s \sqrt{1 - \left(\frac{G_0\omega_s}{2\omega_p}\right)^2} \quad + \quad \frac{G_0\omega_s^{\,2}}{2\omega_p} \tag{5}$$

have a damping term $G_0 \dfrac{\omega_s^2}{2\omega_p}$ provided G_0 is negative. Critical damping is achieved for:

$$\mathrm{Im}\; G(s = j\omega_s) = \frac{G_0\omega_s}{\omega_p} = -2 \quad . \tag{6}$$

2.3 A real differentiator in the feedback path

The ideal differentiator $G(s) = G_0 s/\omega_p$ is not realizable in practice, since it has infinite gain at infinite frequency. The gain must roll off at some frequency $(1/\tau_1) > f_s$. Moreover, the loop gain at the revolution frequency f_{rev} must be small, in order to avoid the excitation of

coupled bunch modes. Therefore a second roll off point at a frequency $(1/\tau_2) < f_{rev}$ must be provided (Fig. 3). This second roll off may indeed be given naturally by the cavity bandwidth itself.

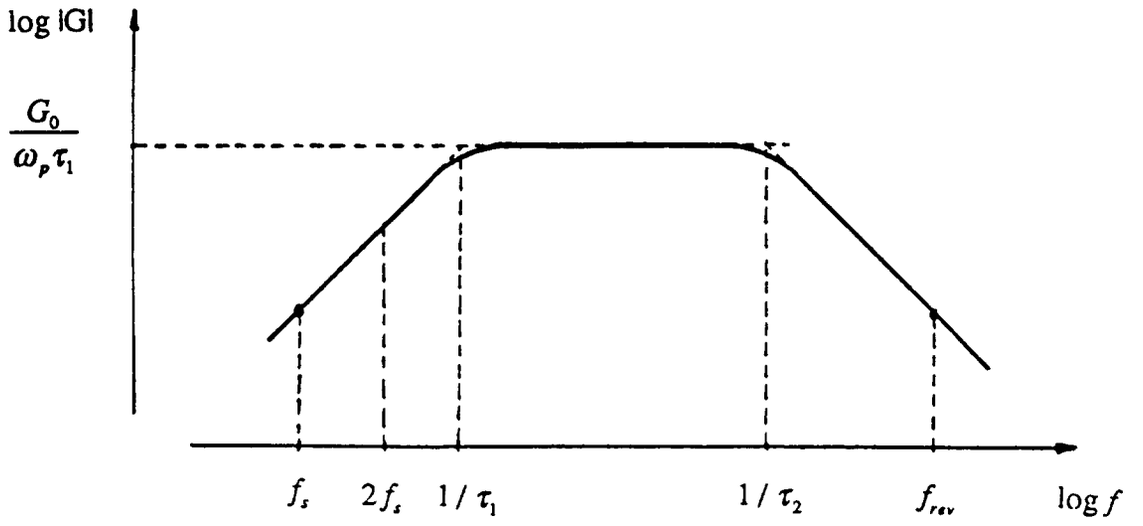

Fig. 3 Frequency response of a real differentiator

The overall transfer function $G(s)$ for a realistic differentiator can be written as:

$$G(s) = \frac{G_0 s}{\omega_p} \quad \frac{1}{1+s\tau_1} \quad \frac{1}{1+s\tau_2} \tag{7}$$

which leads to the characteristic equation:

$$\tau_1\tau_2 s^4 + (\tau_1+\tau_2)s^3 + (1+\omega_s^2\tau_1\tau_2)s^2 + \left(\tau_1+\tau_2-\frac{G_0}{\omega_p}\right)\omega_s^2 s + \omega_s^2 = 0 \quad . \tag{8}$$

The system is stable if all roots of this 4th-degree polynominal have negative real parts. This can be checked without actually solving the characteristic equation by using the Routh-Hurwitz [1] criterion which for a 4th-order equation:

$$a_4 s^4 + a_3 s^3 + a_2 s^2 + a_1 s + a_o = 0$$

can be written:

$$a_4 > 0, \qquad a_3 > 0, \qquad a_2 - \frac{a_1 a_4}{a_3} > 0$$

and:

$$a_1 a_2 a_3 - a_1^2 a_4 - a_3^2 a_0 > 0 \quad .$$

Applied to equation (8), the Routh's inegalities lead to the following conditions:

$$\begin{cases} G_0 / \omega_p > -\dfrac{1}{\omega_s^2}\left(\dfrac{1}{\tau_1}+\dfrac{1}{\tau_2}\right) \\ G_0 / \omega_p > -\dfrac{1}{\omega_s^2}\left(\dfrac{1}{\tau_1}+\dfrac{1}{\tau_2}\right)+(\tau_1+\tau_2) \\ G_0 / \omega_p < 0 \ . \end{cases}$$

The first two conditions impose a limit on the loop gain, which for $\tau_1 >> \tau_2$ can be written:

$$\tau_1 - \frac{1}{\omega_s^2 \tau_2} \ < \ \frac{G_0}{\omega_p} \ < \ 0 \ . \qquad (9)$$

It can be shown that even for the highest possible gain the quantity $\left(\mathrm{Im}\, G(s = j\omega_s)\right)$ is smaller than unity, which means that critical damping cannot be reached in practice.

In conclusion damping with a differentiator circuit is limited in gain; this is particularly true for machines with high Q_s. There is another reason for limiting the gain: at the frequency $2 f_s$, the loop gain should not be large, as the phase detector is never completely insensitive to amplitude fluctuations (quadrupole mode of oscillation of the beam). If the gain is too large the loop may excite the unwanted quadrupole mode.

A variant of the differentiator scheme has been proposed [2, 3] in which the differentiator is replaced by a 90° phase shifter at f_s, based on analog or digital delays. A similar study has been made [3], leading also to the result that the loop gain is limited.

The differentiator scheme can easily be implemented (the DC or slowly varying offsets are automatically rejected); it is well adapted in cases where relatively slow damping is sufficient. In particular it is generally adopted for individual bunch damping in addition to a phase loop, as described in the following section, acting on all bunches at the same time. A typical result [2] is given in Fig. 4, showing the damping of dipole oscillations at injection in PETRA II.

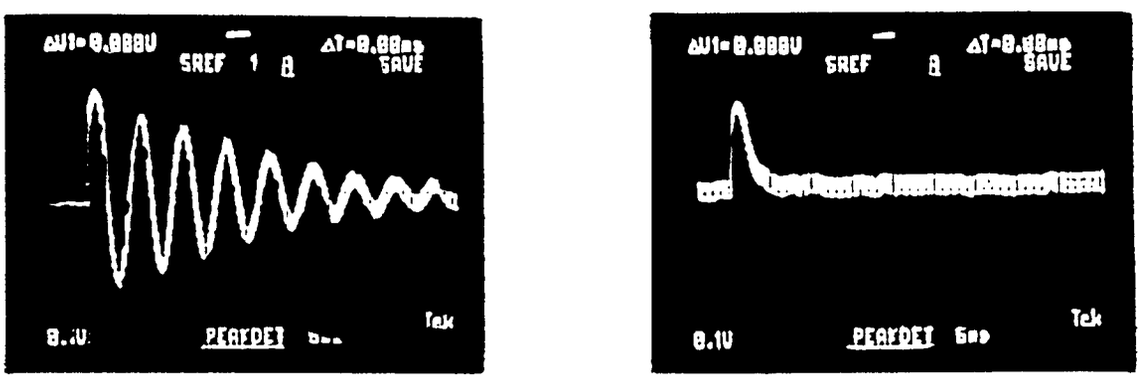

(a) (b)

Fig. 4 Damping of dipole oscillations in PETRA II with differentiator and phase shifter
a) no damping b) with damping

2.4 Feedback path with integrator

The required 90° phase shift at f_s can also be obtained with an integrator in the feedback path, with the transfer function:

$$G(s) = \frac{G_0}{1 + s\tau} \quad . \tag{10}$$

The loop gain at multiples of the synchrotron frequency, as well as at f_{rev} is smaller, as compared to the differentiator case, because the loop gain already rolls off at f_s. Conversely, the loop gain is higher for frequencies below f_s. This is generally an advantage for several reasons:

- the sources of excitation are usually stronger at low frequencies; a higher loop gain is more likely to reduce their effect on the beam.
- the incoherent synchrotron frequency band extends from f_s (for the synchronous particle) downwards. A large gain below f_s will prevent excitation of parts of the beam, especially in the case of long bunches.
- as will be seen in Section 3.2, the coherent synchrotron frequency decreases when the beam intensity increases, making the feedback with integrator better suited for high intensity beams.

The Routh inequalities for a 3rd-order polynominal :

$$a_3 > 0, \qquad a_2 > 0, \qquad a_1 - \frac{a_0 a_3}{a_2} > 0, \qquad a_0 > 0$$

applied to the characteristic equation:

$$\tau s^3 + s^2 + \tau\omega_s^2 s + \omega_s^2(1 - G_0) = 0 \tag{11}$$

lead to the stability criterion:

$$0 < G_0 < 1 \quad . \tag{12}$$

The loop gain is also limited to keep the system stable, and therefore such a scheme is not very interesting as it can only provide weak damping and does not reject the static offsets.

At the gain limit $G_0 = 1$, one of the roots of the characteristic equation (11) becomes $s = 0$: the system gets unstable at a very low frequency. A possible way to overcome the $G_0 < 1$ limitation would be to reduce the overall loop gain at very low frequencies. To achieve this we can measure the beam-cavity phase error instead of the beam-reference phase error, as depicted in Fig. 5. This is equivalent to replacing the beam transfer function B by B-1 in the characteristic equation.

With $B - 1 = -s^2 / (s^2 + \omega_s^2)$, the overall loop gain has a double zero at $s = 0$, as anticipated. The characteristic equation can now be written as:

$$\tau s^3 + (1 + G_0)s^2 + \tau\omega_s^2 s + \omega_s^2 = 0 \quad . \tag{13}$$

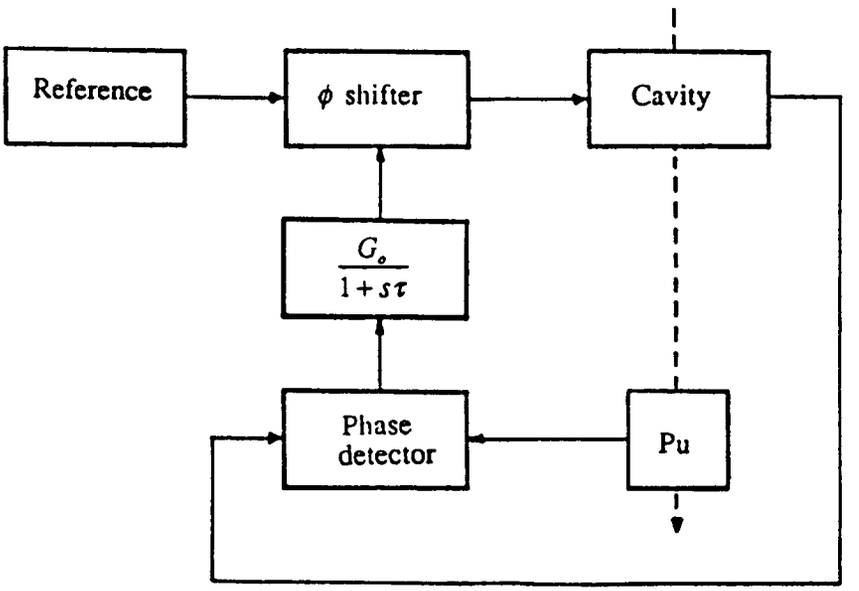

Fig. 5 Damping with integrator and beam-cavity phase measurement

Application of Routh's criterion:

$$\tau > 0; \qquad 1+G_0 > 0; \qquad \frac{G_o \tau \omega_s^2}{1+G_0} > 0; \qquad \omega_s^2 > 0$$

shows that there is no limitation on the loop gain: the system is unconditionally stable. For the more realistic case of a double integrator:

$$G(s) = \frac{G_0}{1+s\tau_1} \quad \frac{1}{1+s\tau_2} \tag{14}$$

in which the term $1/(1+s\tau_2)$ may account for the cavity bandwidth, the result is the same: there is no gain limitation connected with the stability of the system.

Although this scheme with its unlimited gain has the capability of suppressing any dipole motion, it may not be very practical. This is because the large DC gain will amplify considerably any phase detector offsets, thus requiring an unpractically large dynamic range of the phase shifter. A much better solution is to replace this phase shifter by a voltage controlled oscillator (VCO), equivalent to a phase shifter with an infinite range and integrator transfer function ω_p/s (conversion frequency –> phase). The overall transfer function (10) can be restored by having a loop amplifier AC-coupled (transfer function $G_0 s / (1 + s\tau)$).

This scheme: beam-cavity phase detector, AC-coupled amplifier and VCO, is of common use in proton machines [4], provided the VCO stability and linearity are adequate to control the average radial position of the beam. Slowly varying offsets or stable phase variations are automatically rejected by the amplifier AC coupling. If the delays between cavity and phase detector and between pick-up and phase detector are made equal, the slowly varying phase offsets due to RF frequency variations are automatically eliminated.

Such a system has, however, some limitations; for instance if transition has to be crossed, it is easier to control the radial position of the beam directly rather than through the RF frequency (dR/df becomes infinite at transition). In such a case a DC-coupled VCO complemented with additional loops is a possible solution.

2.5 DC-coupled phase loop with radial correction

Assume for the moment that the VCO is driven by a DC-coupled loop amplifier of constant gain G_0.

The characteristic equation:

$$\frac{G_0\omega_p}{s}\,\frac{s^2}{\omega_s^2+s^2}-1=0 \tag{15}$$

$$s^2-G_0\omega_p s+\omega_s^2=0$$

has two roots, one strongly damped, for $|G_0\omega_p| >> \omega_s$ and G_0 negative, and a second one, weakly unstable in the vicinity of $s = 0$. As such, the system is therefore not stable (as expected); a fact which can be also analyzed by looking at its closed-loop response, including beam. If a perturbation Δf_{in} is introduced at the VCO input, the beam frequency deviation Δf_{out} can be calculated, giving the closed loop response:

$$\frac{\Delta f_{out}}{\Delta f_{in}}=\frac{B}{1-G_o\frac{\omega_p}{s}(B-1)}=\frac{\omega_s^2}{s^2+\omega_s^2-G_0\omega_p s}\simeq -\frac{\omega_s^2}{G_0 s\omega_p} \tag{16}$$

for G_0 large.

The closed loop response is that of an integrator ($1/s$). This is because the strong phase loop imposes the beam-cavity phase to be proportional to the perturbation Δf_{in}. For instance, for a constant Δf_{in}, the beam energy increases linearly with time (constant stable phase error), and so does the frequency deviation Δf_{out}. This is just the characteristic of an integrator.

To restore stability we can use an additional loop which measures the beam frequency error (or the radial position of the beam) and corrects the VCO input signal (Fig. 6). In the limit of G_0 large, the response of the overall system becomes simply:

$$\frac{\Delta f_{out}}{\Delta f_{in}}=\frac{1}{1-\frac{G_0 s\omega_p}{G_f\omega_s^2}} \tag{17}$$

where G_f is the radial (or frequency loop) gain. This is just the response of a single-pole low-pass filter with a time response:

$$\tau_f=\frac{G_0\omega_p}{G_f\omega_s^2} \tag{18}$$

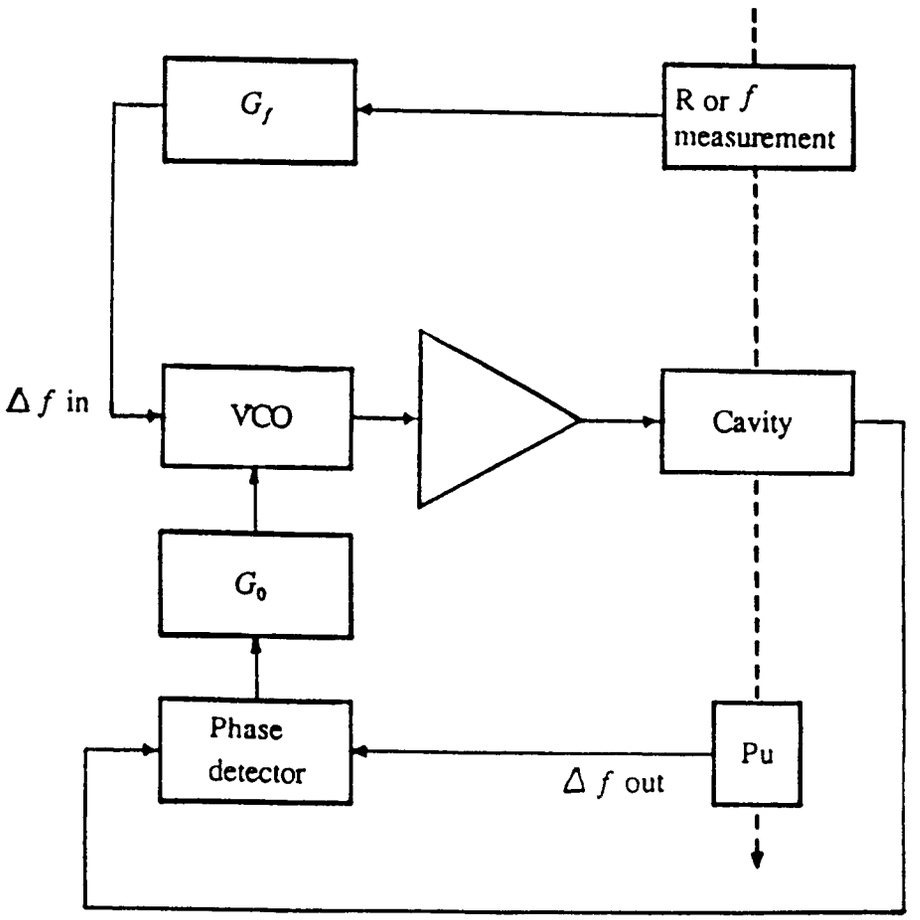

Fig. 6 Damping with phase and radial loops

which, for a large phase loop gain $G_0\omega_p$ and small radial loop gain G_f, can be made much larger than the synchrotron period.

In other words, the perturbations to the overall system (magnetic fluctuations, noise, etc) are filtered and look adiabatic to the beam, as the time constant τ_f can be made very long compared to the synchrotron period (even in the vicinity of transition, where $\omega_s \rightarrow 0$).

The DC-coupled phase loop and radial loop combination has been in use for decades on proton accelerators and storage rings [5, 6]. In addition to providing a strong damping of the coherent dipole mode (which can never be observed with such a system) it gives a convenient way of controlling the radial beam position without precise frequency synthesizers and magnetic field measurements.

If the beam frequency must be synchronized with an external reference, the radial loop can be replaced by a so called "synchronization loop" (Fig. 7). The phase difference between beam and reference is used to correct the input of the VCO. However such a system has two integrators in cascade (frequency-to-phase conversion with the phase detector of the synchronization loop, and phase loop itself) and is therefore sitting at the limit of stability if G_f is purely real (Fig. 8a). To overcome this problem, the classical solution is to introduce a phase advance network in G_f as shown in Fig. 8b, which restores stability.

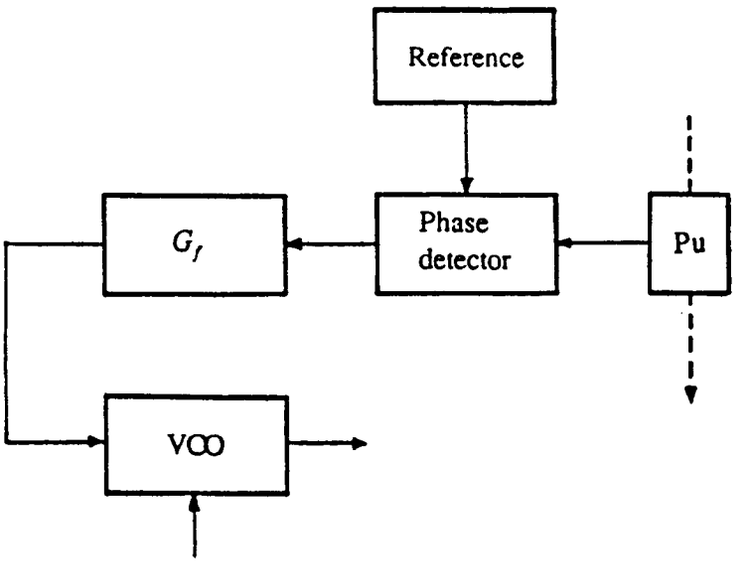

Fig. 7 Synchronization loop

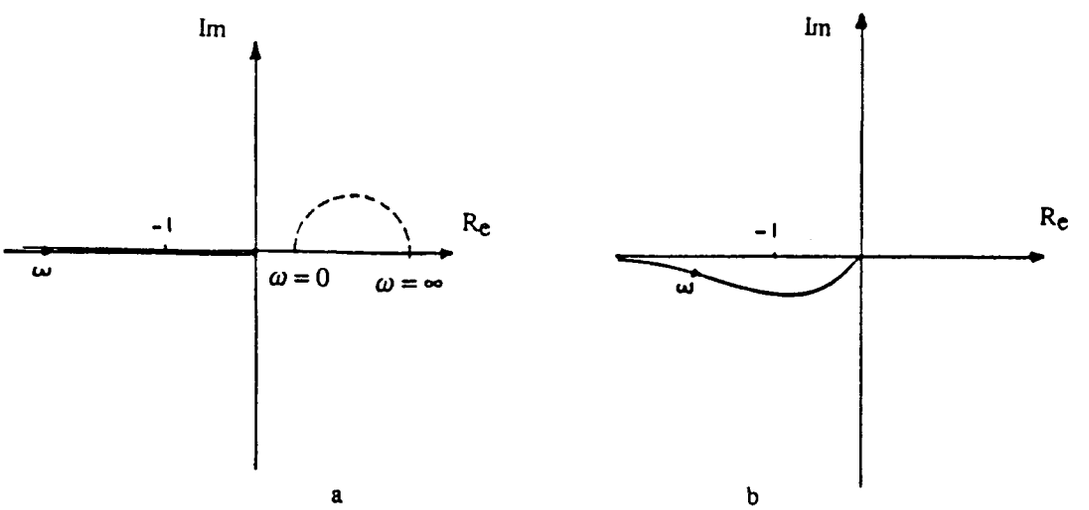

Fig. 8 Open loop transfer function of synchronization loop
a) uncorrected, b) corrected with phase advance network

2.6 Quadrupole-mode damping

Similar methods can be applied to damp the coherent quadrupole mode. The detection of quadrupole oscillations usually relies on the measurement of the peak line density of the bunches. A wide band pick-up electrode followed by a peak detector is the most commonly used technique (Fig. 9). The detector time constant must be long enough to reject components at f_{rev} and higher.

The beam transfer function: amplitude cavity voltage Δ V/V -> quadrupole mode amplitude $\Delta\ell/\ell$ (ℓ = bunch length) is simply:

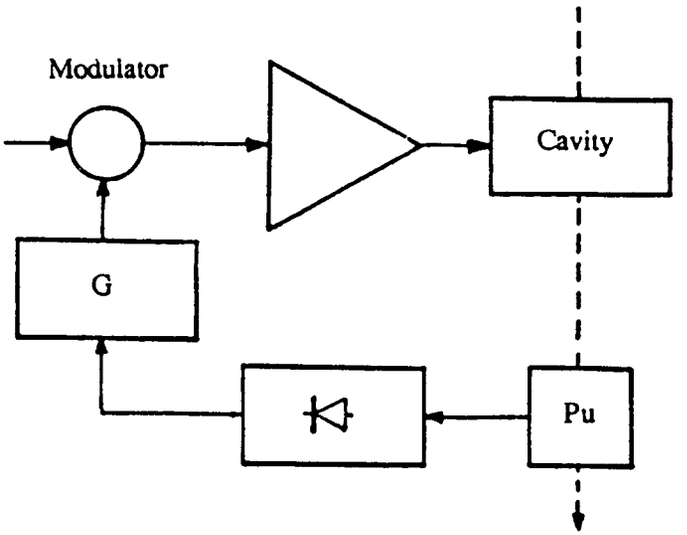

Fig. 9 Quadrupole mode damping

$$B' = \frac{(2\omega_s)^2 \alpha}{s^2 + (2\omega_s)^2} \quad , \tag{19}$$

the factor α depending on the bunch length. In particular, for very short bunches $\alpha = 1/4$.

Damping of the quadrupole mode again requires 90° phase shift at $2f_s$, as for the dipole mode. The differentiator technique is always used, because it automatically rejects the large DC offset of the peak detector (which depends on the bunch intensity and is therefore difficult to compensate).

The gain limitation of the differentiator scheme is generally unimportant, as the quadrupole excitations are usually weak. If $\phi_S \neq 0$, the loop amplifier can also act in the VCO input, and not on the RF modulator [7, 8].

3. HIGH INTENSITY CASE

So far, the influence of the beam current on the accelerating voltage has been neglected. To study the case of high intensity beams, where this effect becomes important, we start with the usual cavity model (Fig. 10), in which the cavity itself, as seen from the accelerating gap, is represented by a lumped-elements RLC circuit. The beam is a pure current source I_B (assuming that the beam energy is much larger than the cavity voltage), and the power generator a second current source I_G. In this model the generator impedance, transformed to the accelerating gap, has been included in the shunt resistance R.

The vector diagram of Fig. 11, at the RF frequency represents the steady state situation in the case of a single cavity (or if all cavities are in phase and identical). The cavity voltage V results from the total current $\vec{I}_T = \vec{I}_G + \vec{I}_B$ flowing into the parallel RLC circuit impedance, characterized by the on-tune current $I_o = V/R$ and the detuning angle ϕ_z ($\tan \phi_z = 2Q\,\Delta f / f_{RF}$, where Q is the cavity quality factor, including generator, Δf the

cavity detuning with respect to the RF frequency f_{RF}). The phase of the beam current $\vec{I}_B$ with respect to $\vec{V}$ is simply $\phi_B + \pi/2$ (below transition case) where ϕ_B is synchronous phase angle determined by independent machine parameters (rate of rise of magnetic field and (or) synchrotron radiation). Our free parameter is the generator phase angle ϕ_L (phase between $\vec{I}_G$ and $\vec{V}$) which can be adjusted via the cavity tuning. The normal operating condition is $\phi_L \simeq 0$, which corresponds to a resistive load to the power generator.

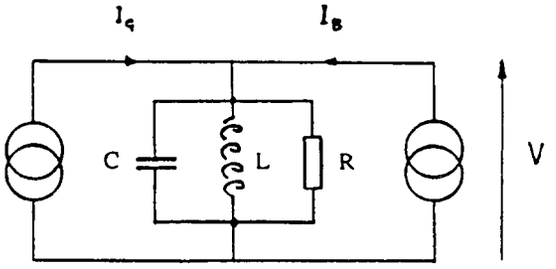

Fig. 10 Lumped circuit equivalent of accelerating cavity

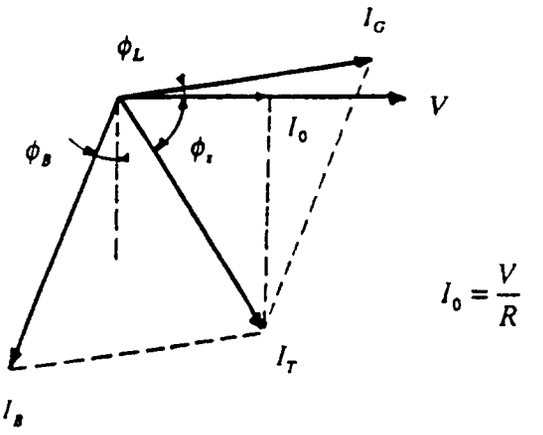

Fig. 11 Steady state vector diagram

3.1 The Pedersen model [9, 10]

In the low intensity case, we have only considered the transfer function from cavity phase (voltage) to beam phase, including the cavity response itself (from $\vec{I}_G$ and $\vec{V}$) in the electronic transfer function. Analysis of the high intensity case is far more complicated, not only because V is now influenced by $\vec{I}_B$, but also because the cavity may be largely detuned giving cross modulations from amplitude to phase and vice-versa.

In the following we shall follow the analysis of F. Pedersen [9]. The variables are the phase and amplitude modulations of $\vec{I}_G$, $\vec{V}$ and $\vec{I}_B$. They are related by the cavity transfer functions G^G and G^B from generator and beam respectively and beam transfer function (B) as shown in Fig. 12. For simplicity we now only consider the case of short bunches, so that the amplitude of I_B is constant, ($I_B = 2I_{DC}$) and the corresponding variable disappears. The transfer function tan ϕ_B comes from the fact that B is the transfer function for phase modulations around the stable phase ϕ_B, which itself depends on the amplitude of $\vec{V}$.

Phase and amplitude modulations can be represented by their two rotating vectors at the modulation frequency. The cavity transfer functions from modulation of $\vec{I}_T$ to modulation of $\vec{V}$ are therefore given by:

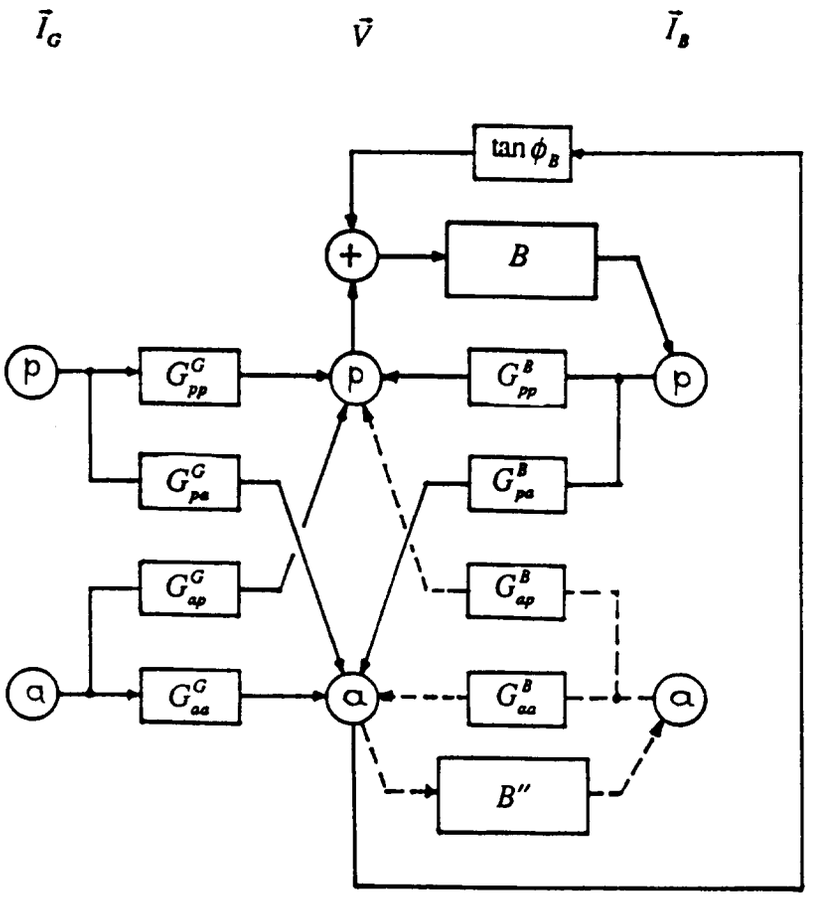

Fig. 12 The Pedersen model

$$G_{pp} = G_{aa} = \tfrac{1}{2}\left\{\frac{Z(s+j\omega_{RF})}{Z(j\omega_{RF})} + \frac{Z(s-j\omega_{RF})}{Z(j\omega_{RF})}\right\}$$
$$G_{pa} = G_{ap} = \tfrac{1}{2}\left\{\frac{Z(s+j\omega_{RF})}{Z(j\omega_{RF})} - \frac{Z(s-j\omega_{RF})}{Z(j\omega_{RF})}\right\} \qquad (20)$$

where G_{pp}, G_{aa} are the transfer functions from phase modulation to phase modulation, or amplitude modulation to amplitude modulation, and G_{pa}, G_{ap} are the transfer functions from phase modulation to amplitude modulation and vice versa. The cavity impedance $Z(s)$ is given by:

$$Z(s) = \frac{2\sigma R s}{s^2 + 2\sigma s + \omega_r^2} \qquad (21)$$

where $\sigma = \omega_r / 2Q$ is the half cavity bandwidth (in rad/s) and ω_r the cavity resonant frequency. ω_r is related to the detuning angle by:

$$\omega_r = \omega_{RF} + \sigma \tan \phi_z \quad . \tag{22}$$

Combining equations (20) and (21) one finds:

$$G_{pp} = \frac{\sigma^2\left(1+\tan^2\phi_z\right)+\sigma s}{s^2+2\sigma s+\sigma^2\left(1+\tan^2\phi_z\right)} \tag{23}$$

$$G_{pa} = \frac{\sigma \tan\phi_z\, s}{s^2+2\sigma s+\sigma^2\left(1+\tan^2\phi_z\right)} \quad . \tag{24}$$

The final transfer functions from $\vec{I}_B$ and $\vec{I}_G$ to $\vec{V}$ are obtained by projection of the modulations of $\vec{I}_B$ or $\vec{I}_G$ on $\vec{I}_T$ according to:

$$G_{pp}^G = G_{pp}\frac{I_G}{I_T}\cos\left(\vec{I}_T,\vec{I}_G\right) \quad + \quad G_{pa}\frac{I_G}{I_T}\sin\left(\vec{I}_T,\vec{I}_G\right) \tag{25}$$

and similar relations for G_{pa}^G, G_{pp}^B and G_{pa}^B, etc. Finally one obtains the complete transfer functions:

$$\left.\begin{aligned}
G_{pp}^G &= \frac{\sigma^2\left(1+\tan^2\phi_z+Y\left(\sin\phi_B-\tan\phi_z\cos\phi_B\right)\right)+\sigma\left(1+Y\sin\phi_B\right)s}{D} \\
G_{pa}^G &= \frac{-\sigma^2 Y\left(\cos\phi_B+\tan\phi_z\sin\phi_B\right)+\sigma\left(\tan\phi_z-Y\cos\phi_B\right)s}{D} \\
G_{pp}^B &= \frac{Y\left(\sigma^2\left(\tan\phi_z\cos\phi_B-\sin\phi_B\right)-\sigma\sin\phi_B s\right)}{D} \\
G_{pa}^B &= \frac{Y\left(\sigma^2\left(\tan\phi_z\sin\phi_B+\cos\phi_B\right)+\sigma\cos\phi_B s\right)}{D} \\
D &= s^2+2\sigma s+\sigma^2\left(1+\tan^2\phi_z\right) \qquad Y = I_B/I_o \\
G_{aa}^G &= G_{pp}^G \qquad G_{ap}^G = -G_{pa}^G \quad .
\end{aligned}\right\} \tag{26}$$

3.2 System stability without loops

Even without electronic loops built around the RF system, stability is no longer guaranteed at high intensity because of the reaction from the beam to the cavity voltage. If the cavity is driven open loop, as in Fig. 1, there are no modulations on $\vec{I}_G$, neither phase nor amplitude, and therefore Fig. 12 simplifies considerably, leading to the characteristic equation:

$$B\left(G_{pp}^{B} + \tan\phi_B G_{pa}^{B}\right) - 1 = 0 \tag{27}$$

which can be written in polynominal form:

$$s^4 + 2\,\sigma\, s^3 + \left(\omega_s^2 + \sigma^2\left(1+\tan^2\phi_z\right)\right)s^2 + 2\,\sigma\,\omega_s^2 s + \sigma^2\omega_s^2\left(1+\tan^2\phi_z - Y\tan\phi_z / \cos\phi_B\right) = 0 \tag{28}$$

Routh's stability conditions:

$$a_2 - \frac{a_1 a_4}{a_3} > 0$$

and:

$$a_1 a_2 a_3 - a_1^2 a_4 - a_3^2 a_0 > 0$$

applied to (28) lead to the two inequalities:

$$\frac{Y \sin 2\,\phi_z}{\cos\phi_B} < 2 \tag{29}$$

and

$$\tan\phi_z > 0 \tag{30}$$

which are referred to as the Robinson stability limits [11]. The second one (equation 30) is independent of intensity (low intensity limit), whereas the first puts a threshold on the beam current (proportional to Y).

The low intensity limit has often been described in the literature on bunched beam instabilities. The RF cavity is a narrow band resonator whose resistive part may be different for the two synchrotron side bands at $f_{RF} + f_s$ and $f_{RF} - f_s$. Below transition, stability of the n = 0 mode (all bunches in phase) is achieved if $R(f_{RF} + f_s) > R(f_{RF} - f_s)$, which also corresponds to a positive detuning, or $\phi_z > 0$ (Fig. 13).

To interpret physically equation (29) (high intensity limit), let us consider the beam induced voltage $\vec{V}_B = Z\vec{I}_B$ and the generator induced voltage $\vec{V}_G = Z\vec{I}_G$, whose sum $\vec{V}_B + \vec{V}_G$ is simply $\vec{V}$. The corresponding vector diagram (Fig. 14) is the same as the current diagram of Fig. 11 $\vec{I}_B + \vec{I}_G = \vec{I}_T$ but shifted in phase by ϕ_z.

If the quantity tan (ϕ_z - ϕ_L) is evaluated at the stability limit:

$$Y = 2\cos\phi_B / \sin 2\,\phi_z \tag{31}$$

using the relation:

$$\tan\phi_L = \frac{\tan\phi_z - Y\cos\phi_B}{1 + Y\sin\phi_B} \tag{32}$$

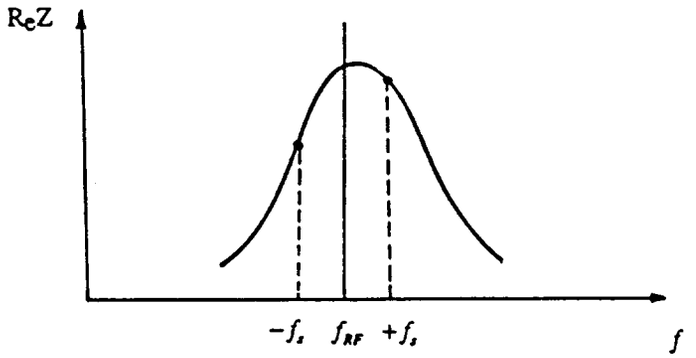

Fig. 13 Low intensity Robinson stability ($R^+ > R^-$ for $\gamma < \gamma_T$)

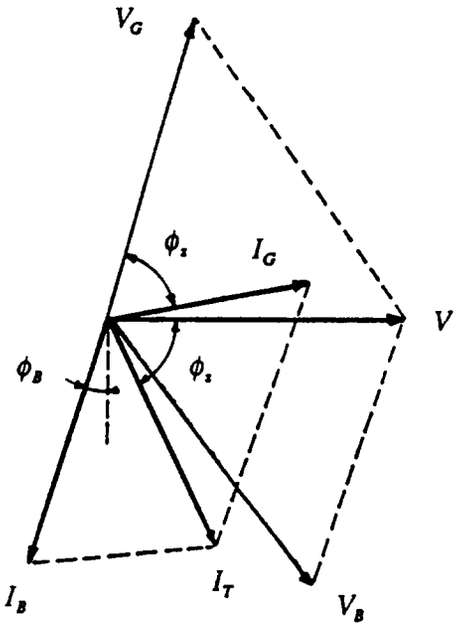

Fig. 14 Vector diagram showing $V = V_B + V_G$

obtained from Fig.11, one easily finds:

$$\tan(\phi_s - \phi_L) = \frac{1}{\tan \phi_B} \tag{33}$$

showing that the vectors $\vec{V}_G$ and $\vec{I}_B$ are in opposition. The stability condition (29) can therefore be interpreted as the limit where the beam sits on the crest of the generator induced voltage. For the coherent dipole motion of the bunch, only this voltage can provide a restoring force (the beam induced voltage simply follows the bunch motion and cannot contribute). Therefore when the vector combination is such that the beam reaches the crest of the generator driven voltage, longitudinal focusing (or stability) is lost for the dipole mode.

The stability limits (29) and (30) are shown on the diagram of Fig. 15, where the dashed areas are forbidden. The curve $\tan \phi_s = 0$ or $Y = \tan \phi_s / \cos \phi_B$, corresponding to a resistive load to the power source is also shown on this diagram.

Combining (31), (32) and the following equation obtained from Fig. 11:

$$I_G = I_0(1 + Y \sin \phi_B) / \cos \phi_L \tag{34}$$

one finds, at the threshold current:

$$I_G = 2\, I_0$$

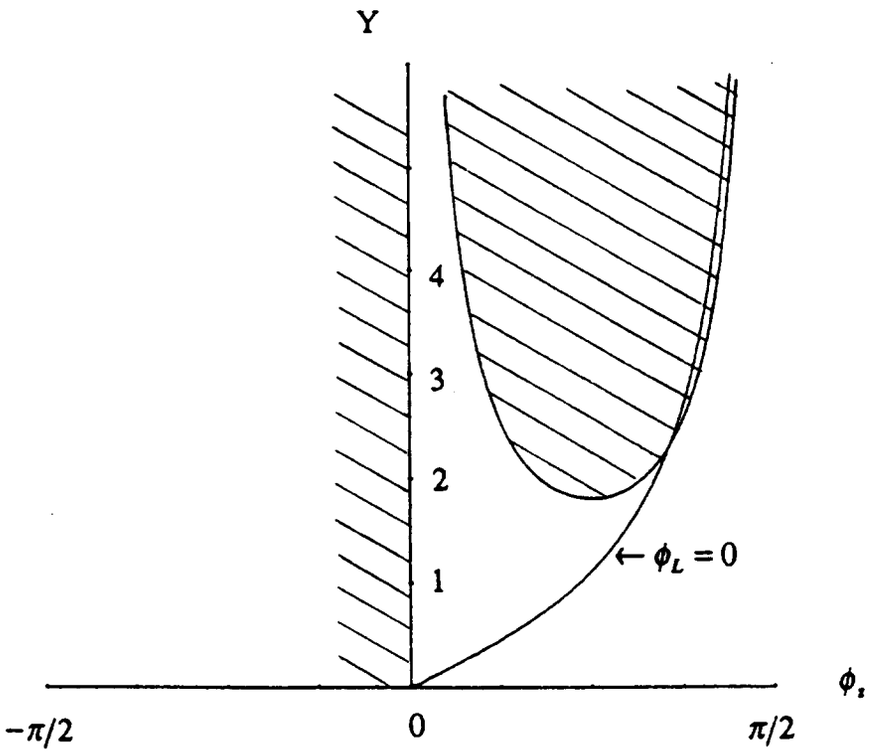

Fig. 15 Robinson stability limits

for the optimum power transfer situation ($\phi_L = 0$). In other words, the power delivered to the beam is just equal to $V^2/2R$ at the current limit. In the case of a current-source-type generator (tetrode, for instance) this corresponds to the power lost in the cavity walls and the tube. If a matched generator is used (klystron and circulator for instance) in conjunction with a lossless cavity (superconducting), when all power is transferred to the beam (matched generator $I_G = 2I_0$), one is sitting just at the stability limit [12].

3.3 The case of long bunches

For long bunches, the amplitude of $\vec{I}_B$ is no longer independent of the amplitude and phase of $\vec{V}$. In the simple case of a stationary bucket $(\phi_B = 0)$, the amplitude of the RF component of I_B depends only upon the amplitude of the RF voltage through a transfer function:

$$B'' = \frac{\alpha' (2\omega_s)^2}{s^2 + (2\omega_s)^2} \tag{35}$$

where α' depends on the bunch length ($\alpha' = 0$ for short bunches, $\alpha' \geq 0$). Note that α' is different from α (§2.6) as it is defined for the RF component of $\vec{I}_B$, and not for the quadrupole mode amplitude.

Conversely the amplitude modulation of $\vec{I}_B$ perturbs the amplitude and phase of $\vec{V}$, via the cavity response. The relevant transfer functions:

$$G^B_{aa} = G^B_{pp} = \frac{Y\,\sigma^2 \tan\phi_z}{D} \tag{36}$$

$$G^B_{ap} = -G^B_{pa} = -\frac{Y\left(\sigma^2 + \sigma s\right)}{D} \tag{37}$$

are valid for $\phi_B = 0$ (Fig. 12, dashed lines). Without electronic loops, the system relations:

$$\begin{aligned} p_B &= B\,p_v = B\,\left(G^B_{pp}p_B + G^B_{ap}a_B\right) \\ a_B &= B'\,a_v = B'\left(G^B_{pa}p_B + G^B_{aa}a_B\right) \end{aligned} \tag{38}$$

lead to the characteristic equation:

$$\left(1 - BG_{pp}\right)\left(1 - B'G_{aa}\right) \;-\; BB'G_{ap}G_{pa} = 0 \quad . \tag{39}$$

A detailed analysis of this case where there is coupling between the dipole and quadrupole mode has been given in Ref. [13], the result being that the Robinson stability limit (29) may be considerably different for long bunches.

3.4 Stability limits with phase loop

Consider again the phase loop of Fig. 6 which provides strong damping in the low intensity case. The diagram of Fig. 12 must be completed by the phase loop path: measurement of the phase difference between $\vec{I}_B$ and $\vec{V}$ and correction via the phase of the generator current $\vec{I}_G$ (Fig. 16). For simplicity assume $\phi_B = 0$, short bunches, and an idealized transfer function: $C_p = \omega_p / s$ for the *VCO*. The characteristic equation can now be written:

$$\left(s^2 + \omega_s^2\right)\left(s^2 + 2\sigma s + \sigma^2\left(1 + \tan^2\phi_z\right)\right) = \omega_s^2\sigma^2 Y \tan\phi_z - \omega_p s\left(\sigma^2\left(1 + \tan^2\phi_z - Y\tan\phi_z\right) + \sigma s\right). \tag{40}$$

Applying again Routh's criterion to this 4th-order equation gives the following sufficient stability conditions for a large loop gain:

$$\phi_z > 0 \qquad Y < \frac{2}{\sin 2\phi_z} \tag{41}$$

$$\phi_z < 0 \qquad Y < \frac{2}{\left|\tan 2\phi_z\right|} \tag{42}$$

as plotted in Fig. 17. Comparing with Fig. 15, the effect of the phase loop is to remove the low intensity Robinson limit ($\phi_z > 0$). In other words, the strong damping imposed by the

phase loop at low beam currents, overrides the small antidamping which would prevail at $\phi_z < 0$.

On the other hand, the high current limit is not affected by the phase loop, as shown by equation (41). This can also be understood in the following way: the high current limit corresponds to $s = 0$, for which the overall phase loop transfer function $(\omega_p / s)\left(s^2 / (\omega_s^2 + s^2)\right)$ vanishes. The phase loop becomes inefficient when the frequency of the dipole mode approaches zero, i.e. when the high current Robinson limit is reached.

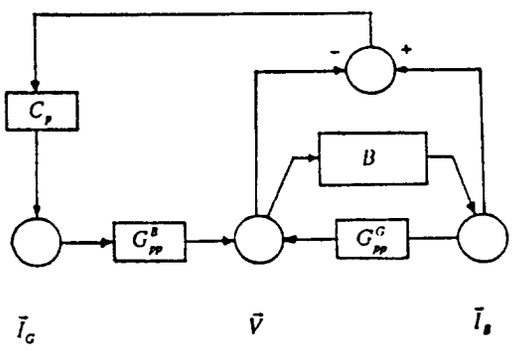

Fig. 16 Phase loop diagram ($\phi_B = 0$)

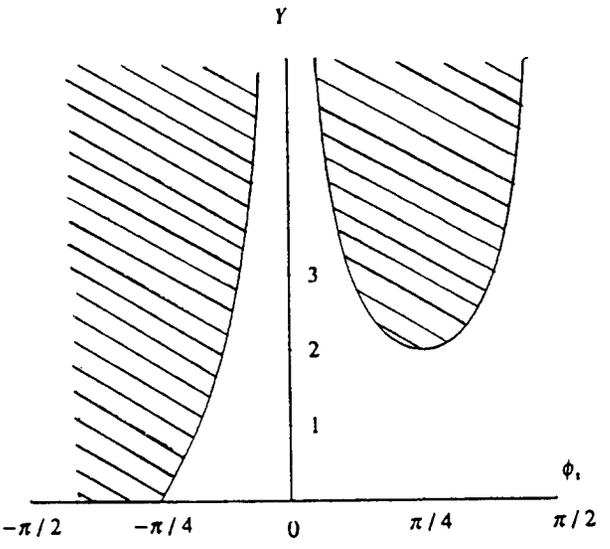

Fig. 17 Robinson stability limits with phase loop ($\phi_B = 0$)

3.5 Complete RF system

In practice a complete RF system comprises, in addition to the phase loop of Fig. 6, a tuning loop to keep $\phi_L = 0$ (static case) and an amplitude loop to regulate the amplitude of V. These loops which are sketched in Fig. 18 can easily be added to the block diagram of Fig. 12. Assuming simple integration type transfer functions for the loop amplifiers (tuning loop $C_T = \omega_T / s$, amplitude loop $C_a = \omega_a / s$), one obtains an 8th-order characteristic equation, which can hardly be treated analytically.

The only simple analytical result known to the author is the following: with tuning and phase loop only (no amplitude loop) Y is limited by the stability condition:

$$Y < \frac{1}{\sin \phi_B} \quad . \tag{43}$$

In the case $\phi_B = 0$, $\phi_L = 0$, σ large, and assuming $B(s) = 0$, Pedersen has derived an analytical criterion [9]:

$$Y < \sqrt{2 + \frac{\omega_a}{\omega_T} + \frac{\omega_T}{\omega_a} + \frac{\omega_T}{\omega_p} + \frac{\omega_a}{\omega_p} + \frac{\omega_p}{\omega_a}} \quad . \tag{44}$$

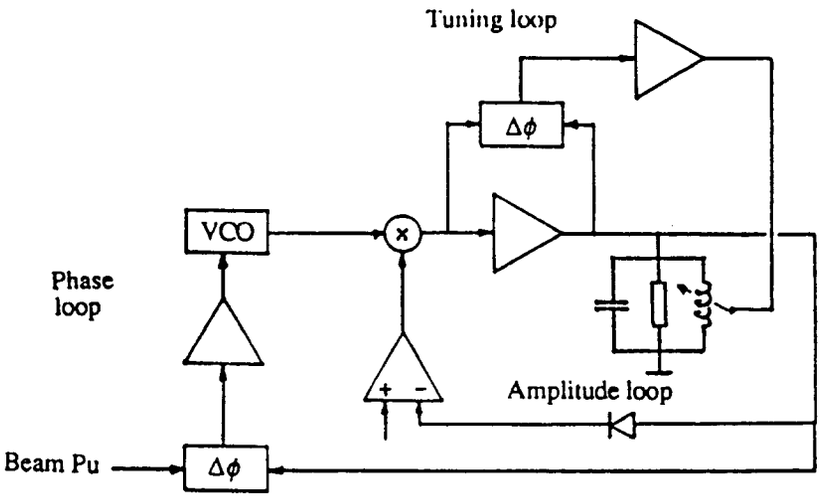

Fig. 18 Schematic of a complete RF system

Numerical solution of the characteristic equation for various values of the parameters leads to stability diagrams like those of Figs. 19, 20 and 21 [14]. When the individual loop bandwidths ω_p, ω_a are equal to σ, the loops are strongly coupled and the stability margin is very small, even at zero beam current (Fig. 19). Separating these frequencies as in Fig. 20 improves the stability margin at $I_B = 0$, but Y is limited to about 2 for the matching condition $\phi_L = 0$. The same result is found in Fig. 21 where ω_p, ω_a are much smaller than σ, giving unconditional stability at $I_B = 0$. There again Y is limited to $Y \simeq 2$ for $\phi_L = 0$.

All these results show that exceeding $Y = 2$ may lead to beam loading instabilities of the RF system, depending on its operating conditions. As a general rule the design condition $Y < 1$, equivalent to:

$$R\ I_b < V \tag{45}$$

provides a reasonable safety margin.

3.6 Cures for heavy beam loading cases

In the situation where the inequality (45) is not satisfied one can try to reduce the parameters I_b or R, as seen by the RF system.

In the so-called "feedforward technique", the power amplifier is driven, not only by the signals generated by the amplitude and phase loops, but by an RF signal derived from a beam monitor. The amplitude and phase of this signal is such that it generates in the cavity a current approximately equal to $-I_B$. From the system dynamics point of view, this is equivalent to reducing the beam current by a large factor (beam loading compensation) [15, 16]. The result is a considerable increase of the stability threshold current. Notice that the static power balance of the RF amplifier is not affected; simply the drive signal from the *VCO* and modulator are now different.

Although this solution is conceptually very simple, it maybe in practice be difficult to implement for various reasons:

- Non linearities of the power amplifier limit the cancellation effect (at best a factor 10 can be achieved in practice), as well as phase and amplitude stability of the various elements in the compensation chain.

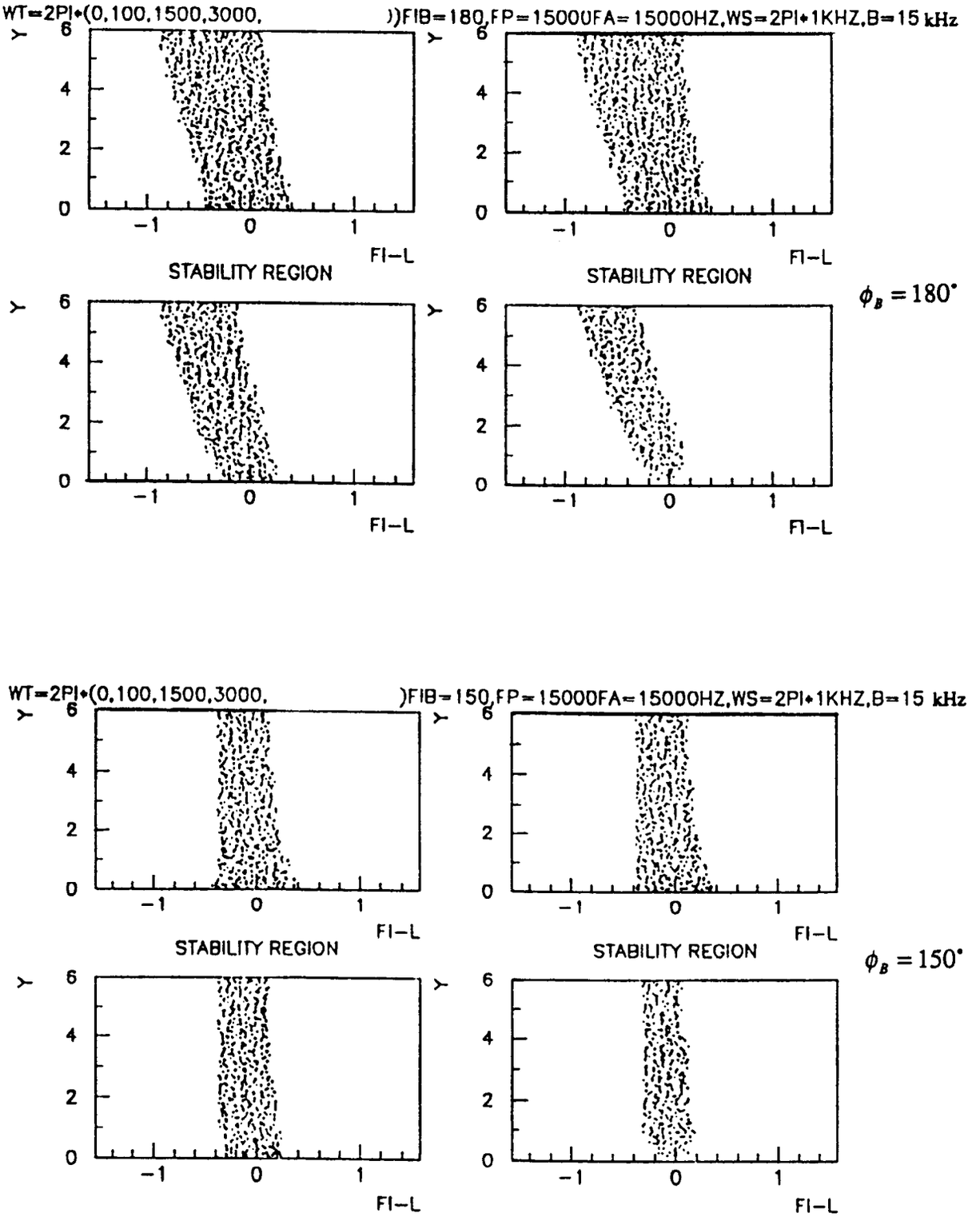

Fig. 19 Stability regions (dotted zones) for complete system and $\omega_p = \omega_a = \sigma$, and for increasing ω_T (0, 100, 1500, 3000 Hz)

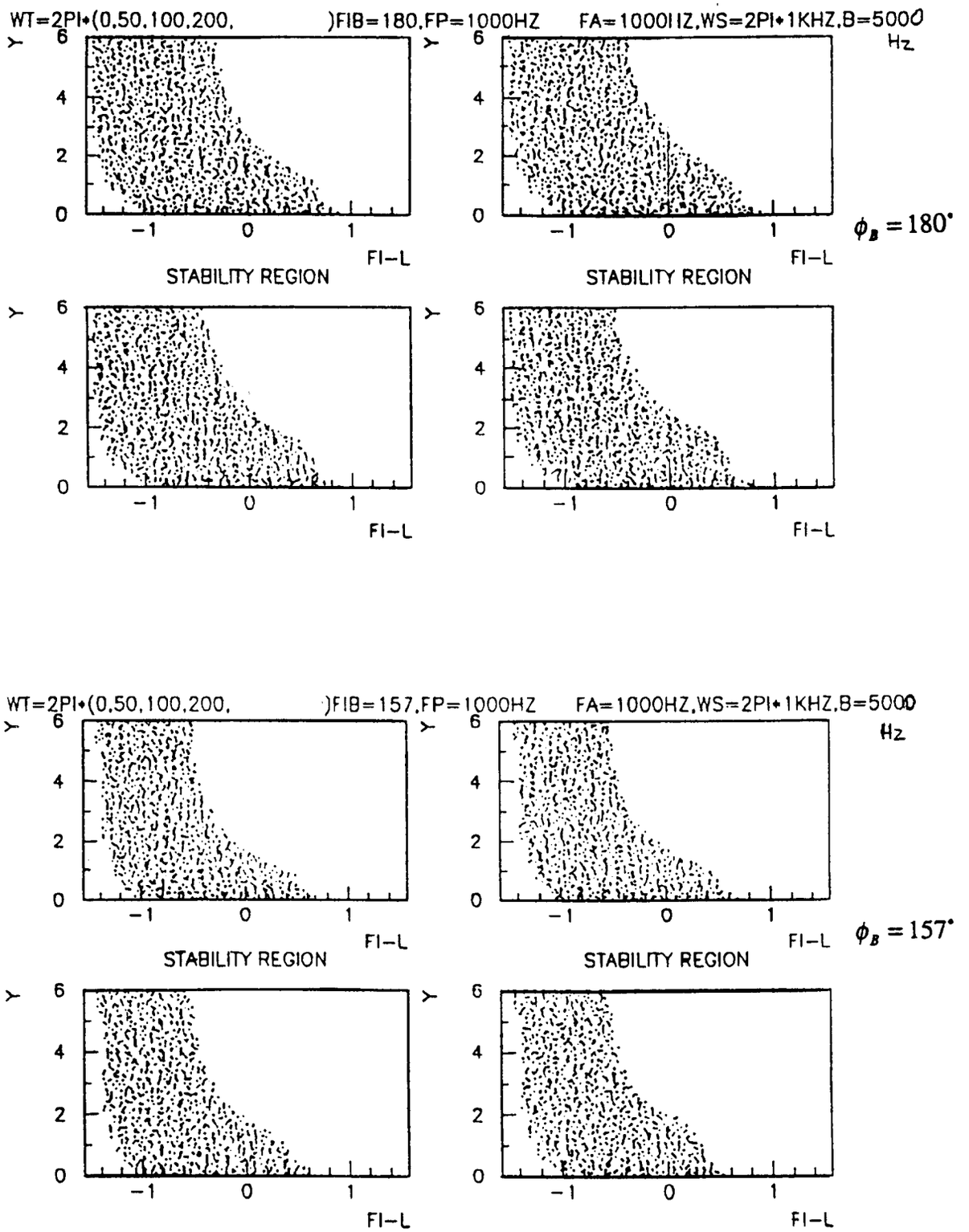

Fig. 20 Same as Fig. 19 but larger cut-off separation ($\omega_p = \omega_a < \sigma$)

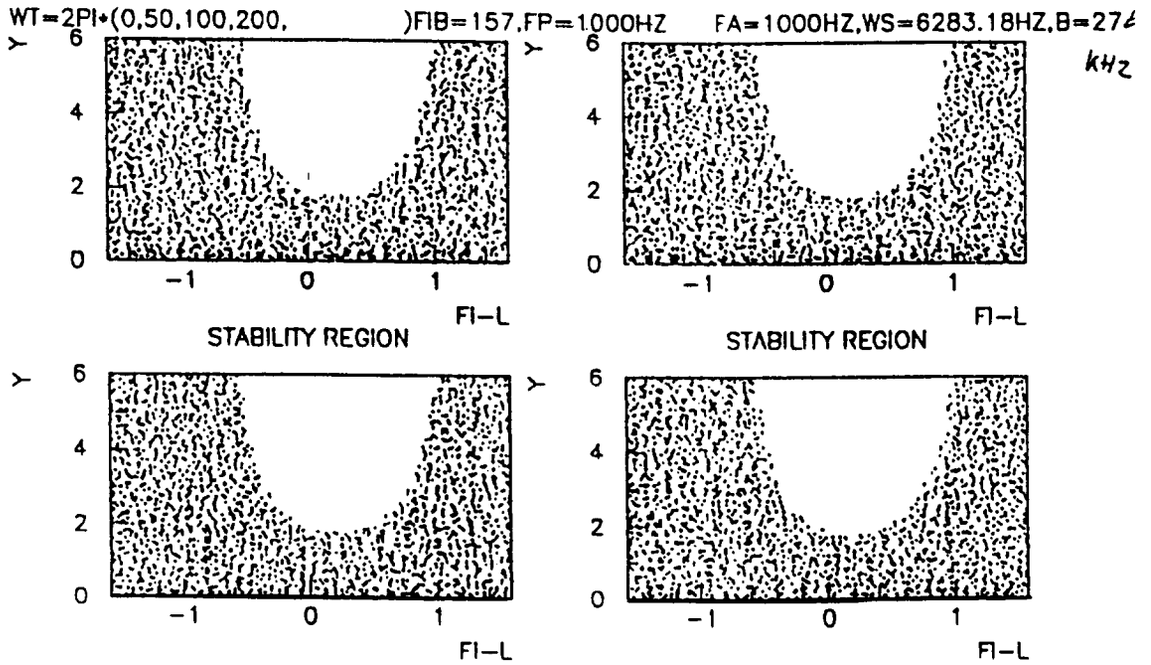

Fig. 21 Same as Fig. 20, but even larger cut-off separation ($\omega_p = \omega_a << \sigma$)

- For a varying RF frequency, all these problems are even more difficult: tolerances on gain and phase are very critical.

- To avoid coupled-bunch effects, the overall delay from beam monitor to cavity should be small, or exactly equal to one turn.

A better, widely used solution, is to use RF feedback around the amplifier, as sketched in Fig. 22. Its effect is equivalent to introducing a shunt resistance across the accelerating gap, whose value is inversely proportional to the loop gain. In such a way R in equation (45) can be reduced by a large factor, increasing in proportion the beam current threshold. For large gains, it can be shown easily that the RF amplifier delivers to the cavity an additional current approximately equal to - I_B, as in the case of the "feedforward technique". However the tolerances on phase and gain are far less critical, provided loop stability is maintained.

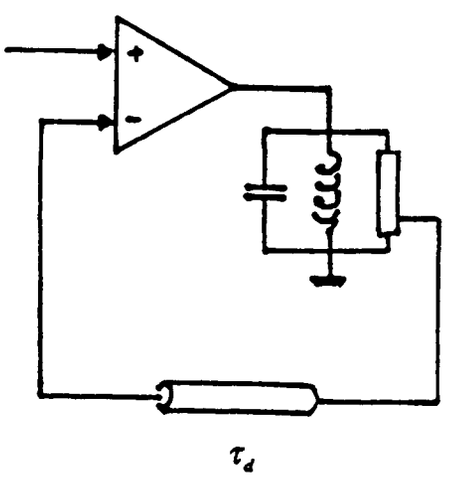

Fig. 22 The RF feedback principle

The overall loop delay τ_d, limits the maximum gain, and therefore the minimum resistance R_{min} which can be achieved with RF feedback. For a reasonable stability margin (45° at unity loop gain), R_{min} can be evaluated easily in the case of a large loop gain. Combining:

- 45° additional phase shift due to τ_d $\quad \delta\omega \ \tau_d = \pi / 4$
- cavity impedance far from resonance $\quad Z \approx \dfrac{R}{2jQ\dfrac{\delta\omega}{\omega_r}}$

one obtains [17]:

$$R_{min} \approx 4\frac{R}{Q}\tau_d \, f_r \ . \tag{46}$$

The cavity half bandwith δf is increased in the same proportion:

$$\delta f = \frac{1}{2} \ \frac{R}{Q} \ \frac{f_r}{R_{min}} \ . \tag{47}$$

At the design limit $R_{min} \cdot I_B = V$ (equation 45), one obtains the ratio of cavity half bandwidth to revolution frequency:

$$\frac{\delta f}{f_{rev}} = \frac{1}{2}\frac{R}{Q} \ \frac{1}{V} \ h \ I_b \tag{48}$$

where h is the harmonic number. If this quantity is small compared to unity, the stability of the RF system only involves modulations of the fundamental RF, as analyzed in the previous sections. This is typically the case of small rings where h is small. For large rings, usually h is larger (several hundreds to several thousands) and $\delta f / f_{rev}$ can be much larger than unity. There the cavity impedance becomes large at the revolution frequency sidebands, and coupled-bunch modes can be strongly excited by the RF system. The parameter $(R/Q)(1/V)$ would be more favourable if superconducting cavities could be employed.

Figures 23 to 25 show a few examples of RF feedback technique applied in various cases: low power, varying frequency around 100 MHz (Fig. 23), high power in the megawatt range (Fig. 24) and superconducting cavity with extremely high feedback gain (Fig. 25). Many more examples are described in the literature [4, 18-22].

Although the equilibrium power conditions are not affected by either feedforward or RF feedback techniques, this is not true during transients, at injection or at the revolution frequency harmonics. In the case of large rings, with slow acceleration rate, this effect may even be dominant and the RF power requirements be determined only by the correction of fast beam loading transients.

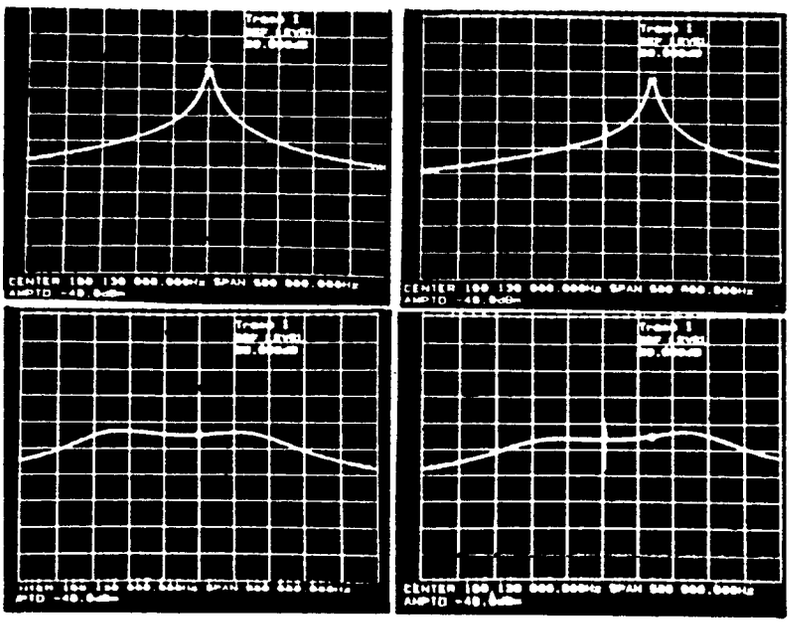

f min f max

Fig. 23
Example of RF feedback
f_{RF} = 100 MHz

frequency swing = 130 kHz
τ_d = 1 μs

loop gain 20 dB
20 kW tetrode amplifier and copper cavity

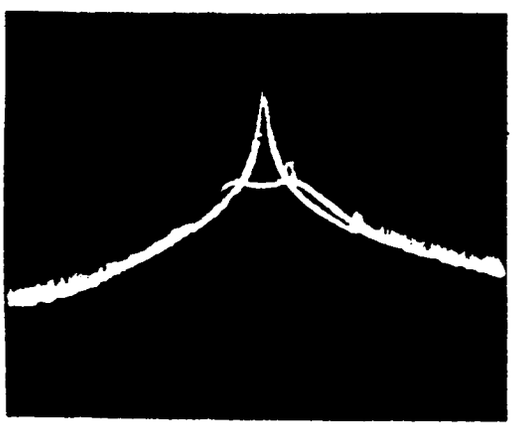

Fig. 24
Example of RF feedback
f_{RF} = 352 MHz

τ_d = 400 μs

loop gain 20 dB

1 MW klystron, circulator, LEP cavity

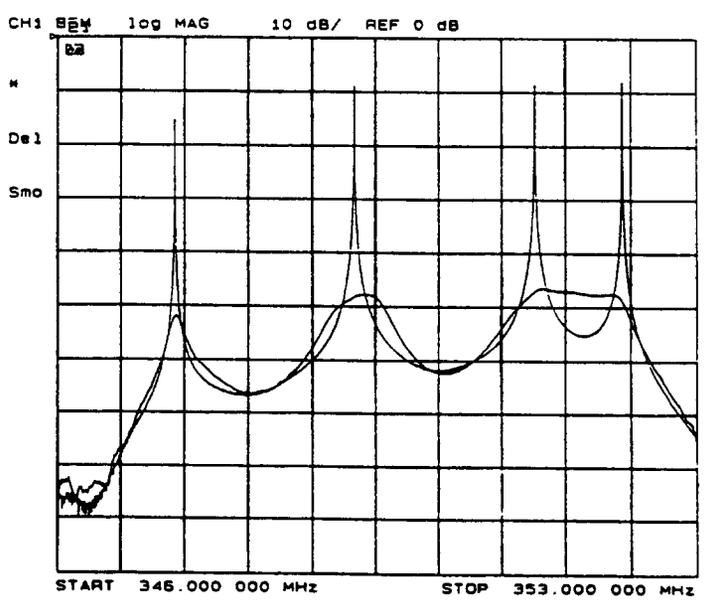

Fig. 25
Example of RF feedback
f_{RF} = 352 MHz

τ_d = 500 μs

loop gain70 dB

50 kW tetrode amplifier no circulator, four-cell LEP superconducting cavity

REFERENCES

[1] E.J. Routh, A treatise on the dynamics of a system of rigid bodies (McMillan, London, 1977).

[2] A. Gamp et al, Damping of coherent synchrotron oscillations occuring at injection of 7.5 GeV protons into PETRA II. EPAC, Nice, June 1990. Editions Frontières, 91192 Gif-sur-Yvette, France

[3] F. Voelker, G. Lambertson, Stability of feedback against coupled bunch motion. Internal note, BECON-77, Berkeley, January 1990.

[4] R. Johnson, S. van der Meer, F. Pedersen, G. Shering. Computer control of RF manipulations in the CERN Antiproton Accumulator, IEEE Trans. Nucl. Sci. NS-30 (4), p 2290, Aug 1983.

[5] W. Schnell, Remarks on the phase lock system of the CERN Proton Synchrotron. Int. Conf. on High Energy Accel. 1959, CERN, Geneva, p. 485-489.

[6] H.G. Hereward, Open and closed loop properties of an RF accelerated beam. Internal Report CERN-PS-4497.

[7] H.G. Hereward, Second order effects in beam control systems of particle accelerators. Proc. 1961, Int. Conf. High Energy Accel, (Broohaven, Nat Lab., Upton, New York, 1961) p. 236-243.

[8] E.C. Raka, Damping bunch shape oscillations in the Brookhaven AGS, IEEE Trans Nucl Sci. Vol NS-16, No. 3, June 1969, p 182-186.

[9] F. Pedersen, Beam loading effects in the CERN PS Booster, IEEE Trans Nucl Sci. Vol NS-22, No. 3, June 1975, p 1906-1909.

[10] F. Pedersen, A novel RF cavity tuning scheme for heavy beam loading, IEEE Trans Nucl. Sci. Vol NS-32, No.5, Oct. 1985, p 2138-2140.

[11] K.W. Robinson, Stability of beam in radiofrequency system, Internal Report CEAL-1010, Feb 1964, Cambridge Electron Accelerator.

[12] E. Haebel, Superconducting cavity matching and the Robinson instability limit, Internal note CERN/EF/RF 89-2 (1989).

[13] Tai-Sen F. Wang, Bunched beam longitudinal mode coupling and Robinson type instabilities, Particle Accelerators Vol. 34, p.105, 1990.

[14] Qin Jiu, Institute for High Energy Physics Acad. Sinica. Beijing. Private communication.

[15] D. Boussard et al, Collective effects at very high intensity in the CERN PS, IEEE Trans Nucl. Sci. Vol NS-26, No.3, June 1979, p. 3568.

[16] P. Barratt et al, RF system and beam loading compensation on the ISIS synchrotron, EPAC, Nice, June 1990, Editions Frontières, 91192 Gif-sur-Yvette, France

[17] D. Boussard, Control of cavities with high beam loading, IEEE Trans. Nucl. Sci. Vol NS-32, No.5, Oct 1985, p. 1852.

[18] R. Garoby et al, RF system for high beam intensity acceleration in the CERN PS, Proc. 1989 IEEE Part.Accel. Conf. Chicago, Argonne Nat. Lab. editor, p. 135.

[19] J-M. Baillod et al, A second harmonic (6-16 MHz) RF system with feedback reduced gap impedance for accelerating flat-topped bunches in the CERN PS Booster, IEEE Trans. Nucl. Sci. Vol NS-30, 1983, p. 3499.

[20] D. Boussard et al, The 100 MHz RF system for the CERN collider, EPAC, Rome, June 1988, World Scientific, Singapore, 1988, p. 991.

[21] D. Boussard, H.P. Kindermann, V. Rossi, RF feedback applied to a multicell superconducting cavity, ibid, p. 985.

[22] S.T. Craig, R.J. West, Beam loading compensation for 52 MHz RF systems, EPAC Nice, June 1990, Editions Frontières, 91192 Gif-sur-Yvette, France